Noname manuscript No.
(will be inserted by the editor)

Supplementary Material: Formation mechanisms of macroscopic globules in andesitic glasses from the Izu-Bonin-Mariana forearc (IODP Expedition 352)

Raúl O. C. Fonseca[1] · **Lina T. Michely**[2] · **Maria Kirchenbaur**[3] · **Julie Prytulak**[4] · **Jeffrey Ryan**[5] · **Kerstin Hauke**[6] · **Felipe P. Leitzke**[7] · **Renat R. Almeev**[3] · **Chris S. Marien**[8] · **Axel Gerdes**[9] · **Rico Schellhorn**[6]

the date of receipt and acceptance should be inserted later

1 Raman spectroscopy and X-ray diffraction

To identify the mineral assemblage in each textural unit, single spot measurements were conducted with a high resolution Horiba Scientific HR800 confocal Raman system equipped with an Olympus BX41 microscope and an electron-multiplier CCD detector. An external silicon standard was used during auto calibration. To correct for any spectrometer shift during measurements, the intense Ne line at 585.24878 (± 0.00005) nm (Saloman, 2006) that occurs at a Raman shift of 1707.06 cm^{-1} in the spectra was continuously monitored by placing a Ne lamp alongside the beam path of the scattered light. A 600 grooves/mm grating was used to increase signal intensities and to minimize the number of windows being measured. A long-working distance objective (100×) was used during calibration and measurement. Lasers with different wavelength (784, 633 and 532 nm) were chosen to minimize the fluorescence background for each textural area (andesitic groundmass, globules and interface). For measurements carried out in the interface the laser intensities had to be reduced in order to prevent sample destruction. During signal acquisition the whole spectrum of wave numbers from 100 to 4000 cm^{-1} was covered in order to detect OH or H_2O bands, if there is water present. Under specific circumstances a limited wave number range was chosen to minimize the number of windows in order to increase signal quality at the measuring time. All measurement settings are given together with the raw spectra depicted in Supplementary figures S1 and S2. Data treatment was performed using the open source software fityk (Wojdyr, 2010). Reference spectra were taken from the RRuf database (Lafuente et al., 2016).

In order to quantify the proportions of glass to minerals, as well as to confirm the mineral identification based on other methods (i.e. EMPA and Raman spectroscopy), aliquots of each sample were crushed and globule and glass fragments were handpicked. The the isolated fragments of each phase were ground to a grain size of 1-10 μm and were subsequently evenly distributed on a quartz monocrystal sample carrier. The analysis was performed with a Siemens D-5000 X-ray diffractometer, using a Cu-Kα (1.5418) source (40 kV, 40 mA), a graphite secondary monochromator, and a scintillation

✉ Raúl O. C. Fonseca, Institut für Geologie, Mineralogie und Geophysik, Ruhr-Universität Bochum, E-mail: raul.fonseca@rub.de
· [1] Institut für Geologie, Mineralogie und Geophysik, Ruhr-Universität Bochum, 44801 Bochum, Germany
· [2] Agroislab GmbH, Prof.-Rehm-Str. 6, D-52428 Jülich, Germany
· [3] Leibniz Universität Hannover, Institut für Mineralogie, 30167 Hannover, Germany
· [4] Department of Earth Sciences, Durham University, Science Labs, Durham DH1 3LE
· [5] School of Geosciences, University of South Florida, Tampa, USA
· [6] Institut für Geowissenschaften, Universität Bonn, Meckenheimer Allee 169, 53115 Bonn, Germany
· [7] Laboratório de Geologia Isotópica, Universidade Federal do Rio Grande do Sul, Av. Bento Gonçalves, 9500 Porto Alegre, RS, Brasil
· [8] Institut für Geologie und Mineralogie, Universität zu Köln, 50674 Köln, Germany · [9] Institut für Geowissenschaften, Frankfurt Isotope and Element Research Center (FIERCE), Goethe Universität Frankfurt, Altenhöferallee 1, 60438 Frankfurt am Main, Germany

detector. The scans were performed at room temperature using a step scan of 0.02°, with a recording time of 15 s for each step. Mineral phase identification was performed via DIFFRAC.EVA (Bruker Software). The quantitative estimates of the mineral phases were acquired with TOPAS, a Rietveld-analysis based Bruker Software.

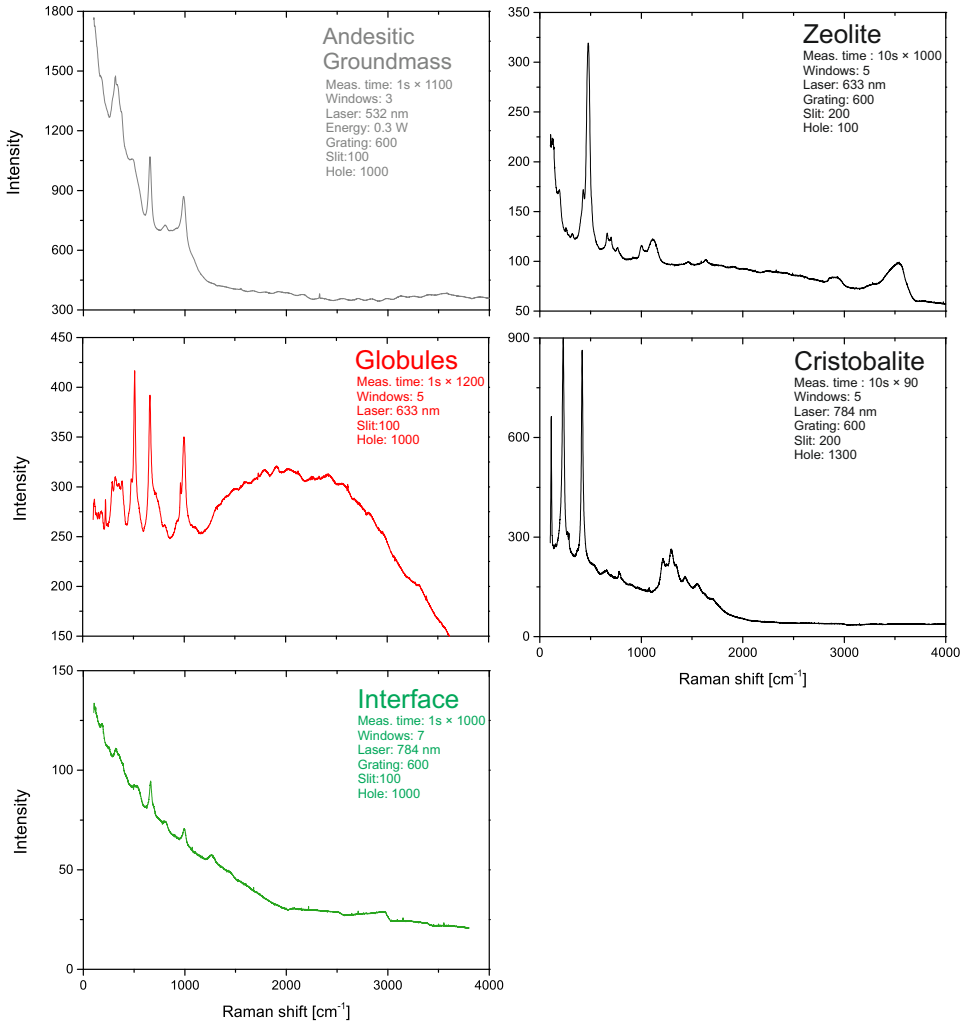

Supplementary figure S 1: Raman spectroscopy: Raw spectra.

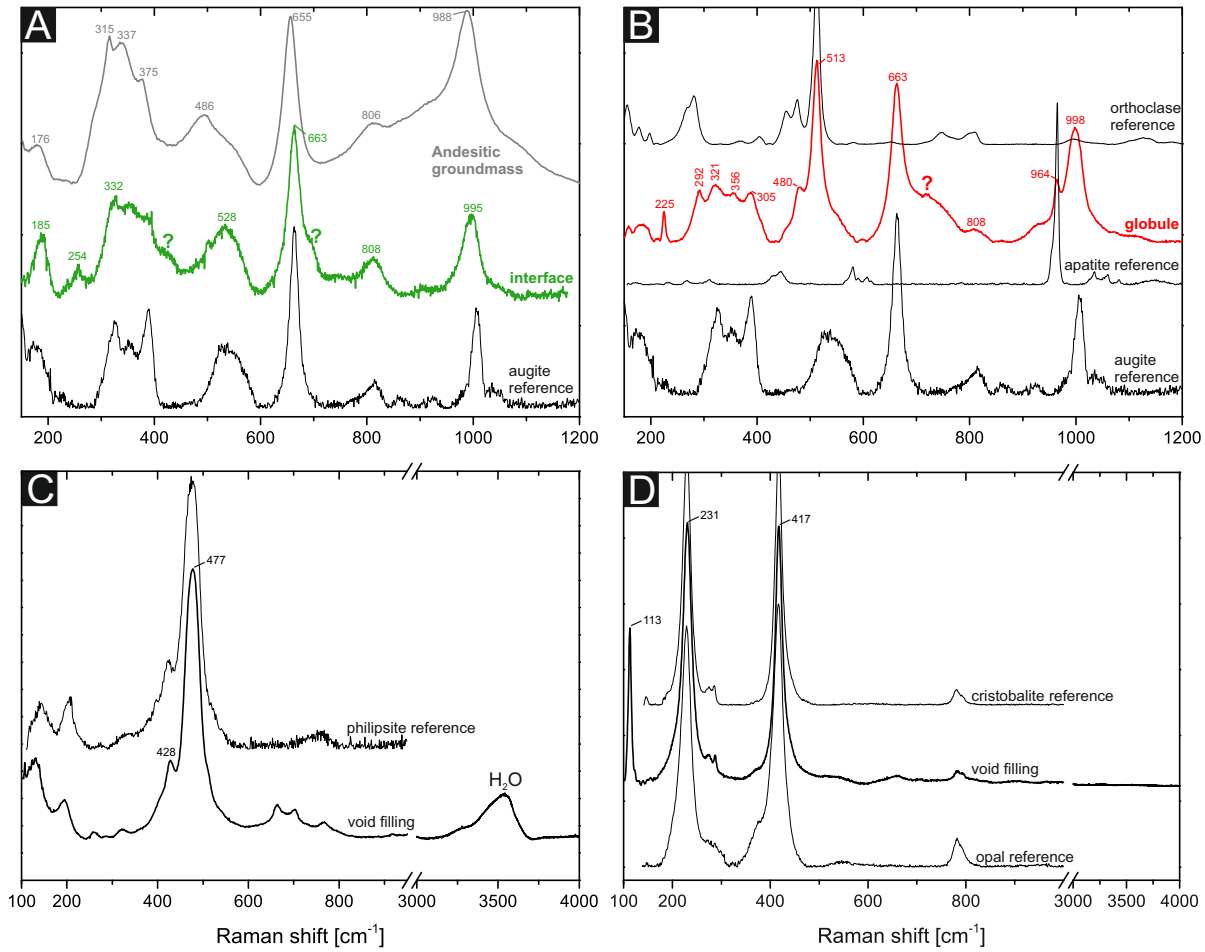

Supplementary figure S 2: Measured Raman spectra from the different textural areas and the voids, displayed with reference spectra from the RRuff database (Lafuente et al., 2016). **A)** Spectrum from the interface and the andesitic groundmass together with an augite reference. **B)** Spectrum from the globule interior, displayed together with an orthoclase, augite and apatite reference. The band at around 964 cm^{-1} is best explained by the presence of apatite (CaF) as a minor mineral phase. **C)** Spectrum recorded from the void-filling minerals. The bands of the recorded spectrum overlap with those from a phillipsite reference. **D)** Spectrum recorded from the void filling, which overlaps with a cristobalite and opal reference. Because, the spectra does not display a visible Raman band of H_2O, cristobalite is the most likely mineral phase. For high quality reference spectra of cristobalite and opal with different H_2O-contents see Ilieva et al. (2007). Reference spectra recorded by Ilieva et al. (2007) also display the sharp band at 113 cm^{-1}).

2 Supplementary Microphotographs of the Izu-Bonin globular samples

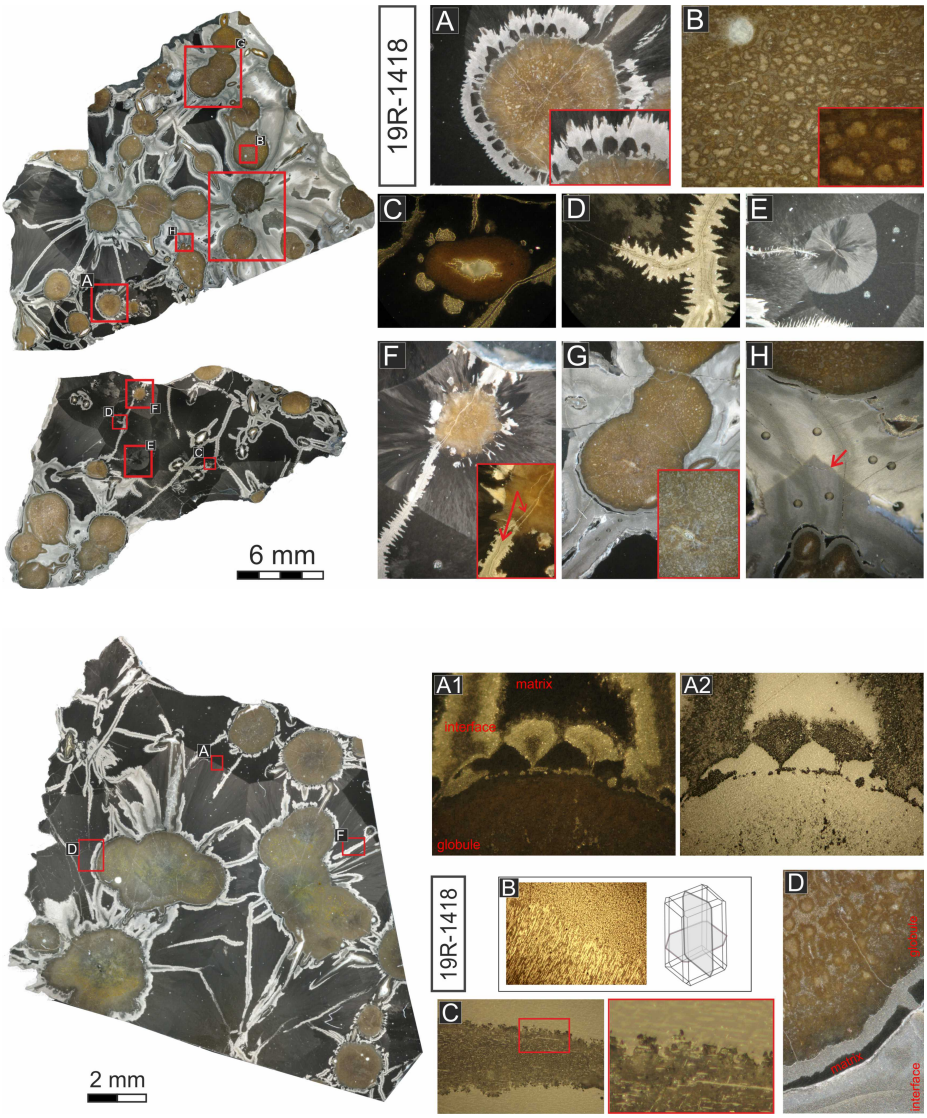

Supplementary figure S 3: Reflected light microscopy: Image panel of Sample 19R-1418 (top half) and sample 19R-6466 (bottom half) .

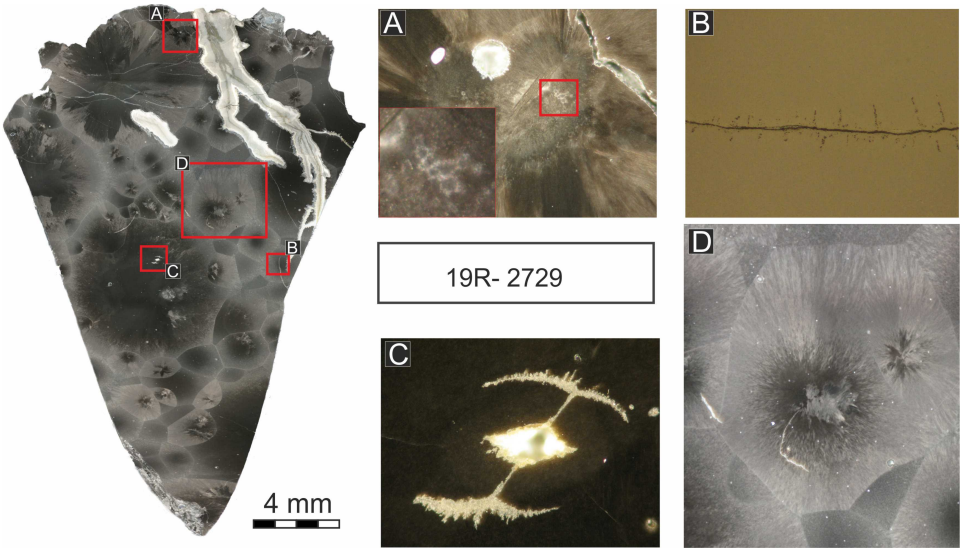

Supplementary figure S 3: Reflected light microscopy: Image panel of Sample 19R-2729.

3 Major element variations of the textural units of the Izu Bonin globular andesites

The major element variations between the main textural units of the Izu-Bonin globular andesites are summarized and displayed in Figure S6 as the variation relative to the andesitic groundmass in wt. %, in a transect across the interface (Figure S7), as well as qualitatively in the X-ray maps (Figure S8). For example, while CaO shows a homogeneous distribution in all textural units most of the other major elements show distinct variations, in at least one of these main units, i.e. globule or interface. The decoupling of Na_2O and K_2O between glass, globules and interface is especially noteworthy (see Table 1 in main manuscript)and also the internal redistribution of FeO, but also SiO_2, Al_2O_3 and K_2O in the orbs of the globules (Figure S8). From the minor elements Cl is the most affected in that it is depleted in the interface and the globules relative to the andesitic groundmass by a factor of ten or more (Figure S6). Phosphorus also shows considerable variations (a factor of three between interface and andesitic groundmass). Evaluated quantitative line scans showing the element variations linked to a change in the textures can be found in the supplement Figure S7.

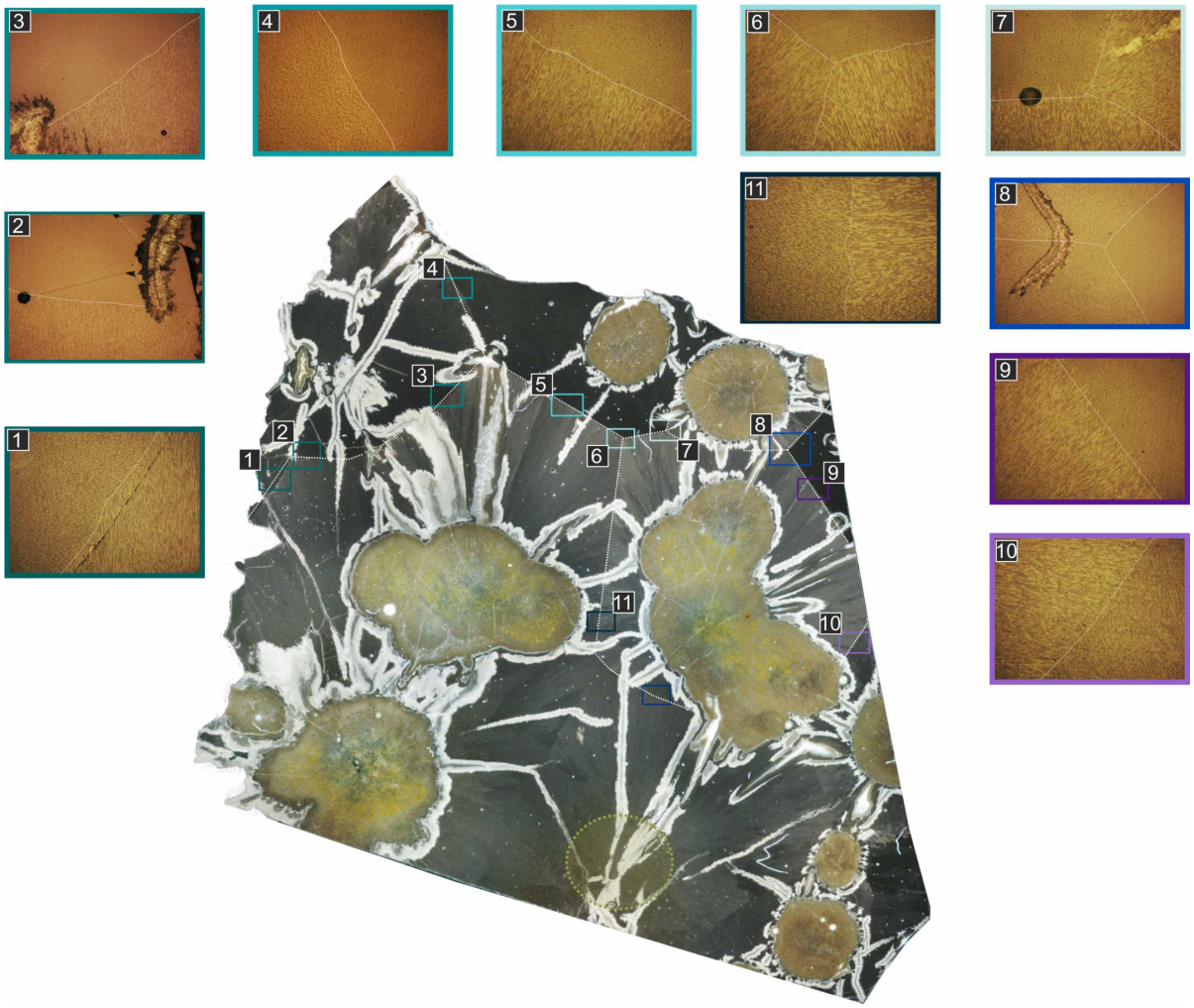

Supplementary figure S 4: Close-up images of the crystallite orientation.

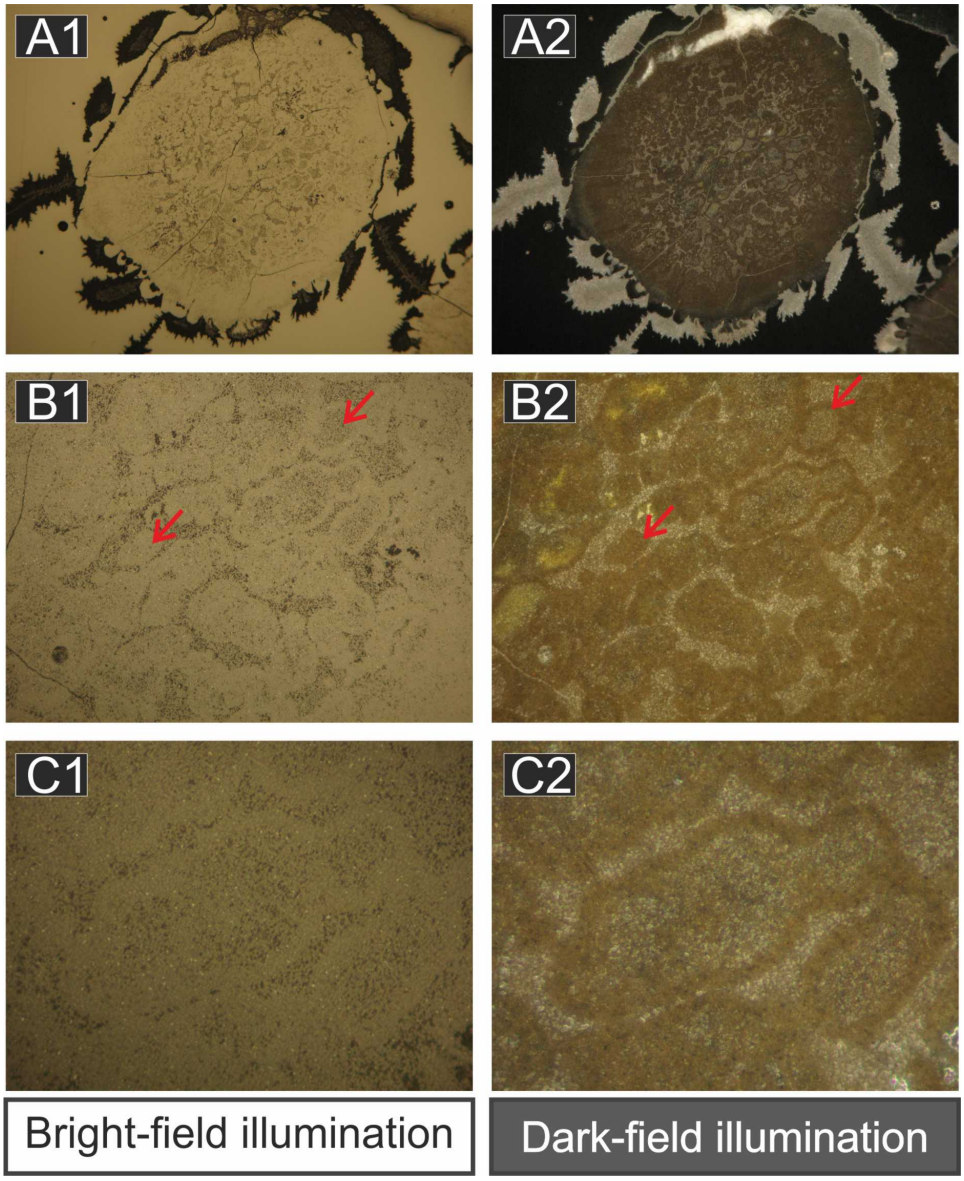

Supplementary figure S 5: Reflected light microscopy: Optical micrographs of globules in both dark and bright field imaging

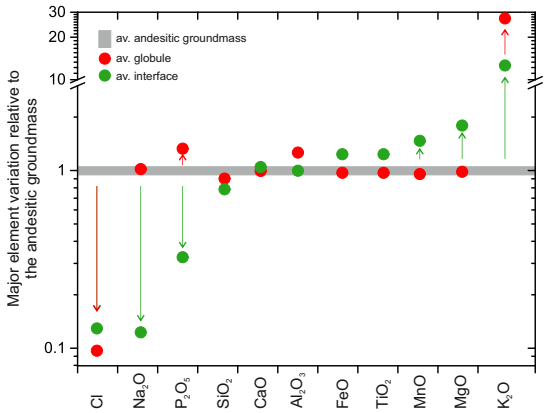

Supplementary figure S 6: Enrichment-depletion diagram: Major and minor element variation relative to the andesitic groundmass.

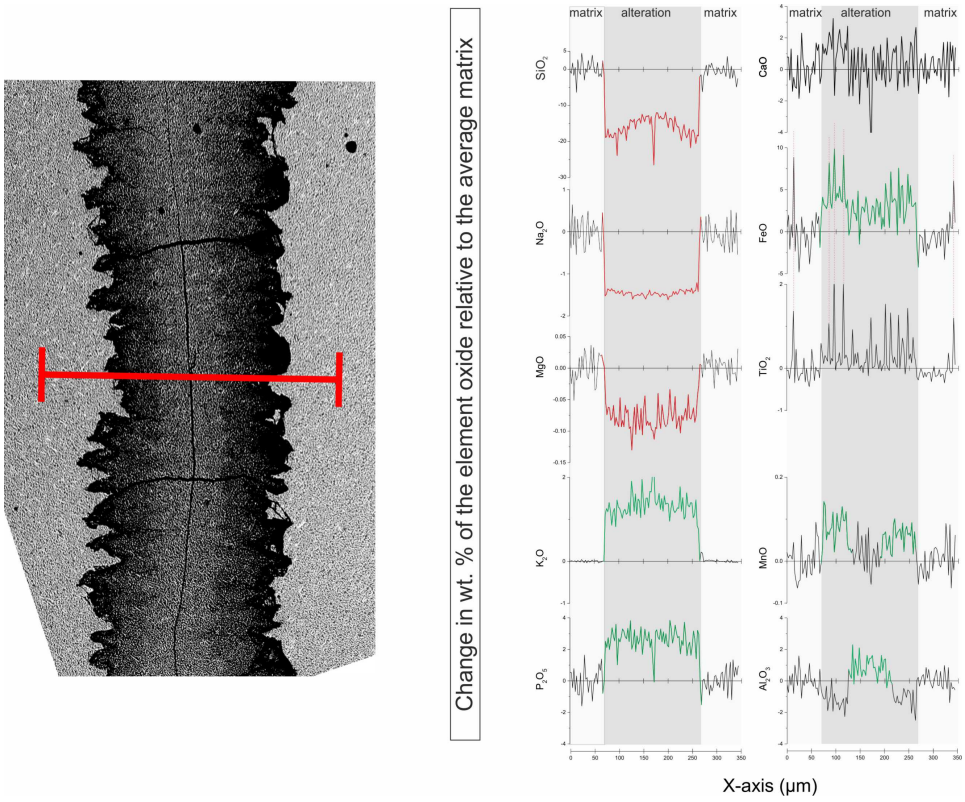

Supplementary figure S 7: Major and minor element abundance variations along a transect of an interface vein.

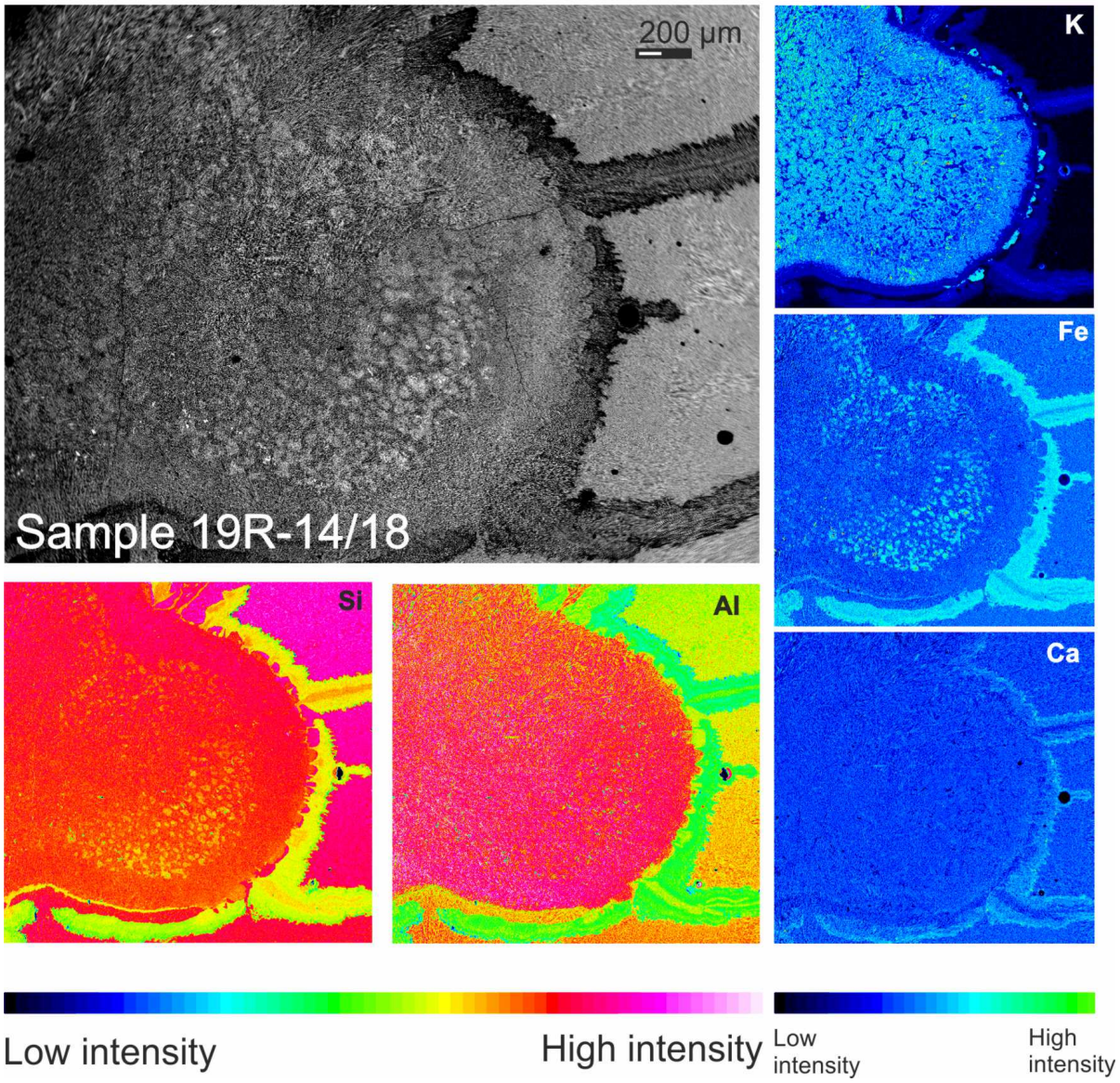

Supplementary figure S 8: Qualitative element distribution map.

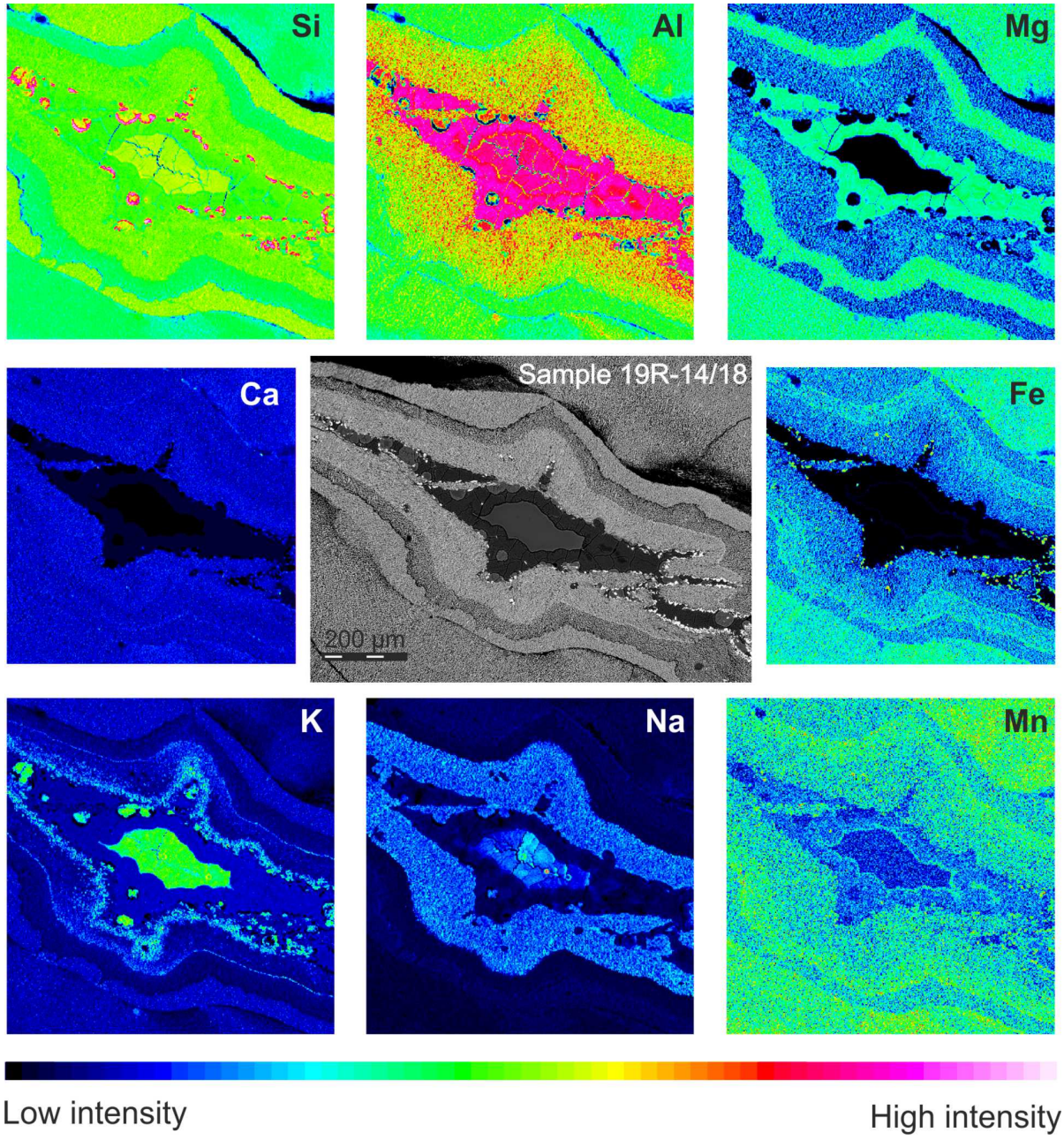

Supplementary figure S 9: Qualitative element distribution map of voids and their mineral fillings

4 Spherulitical crystallization in Unit 6 andesites from borehole 1440B

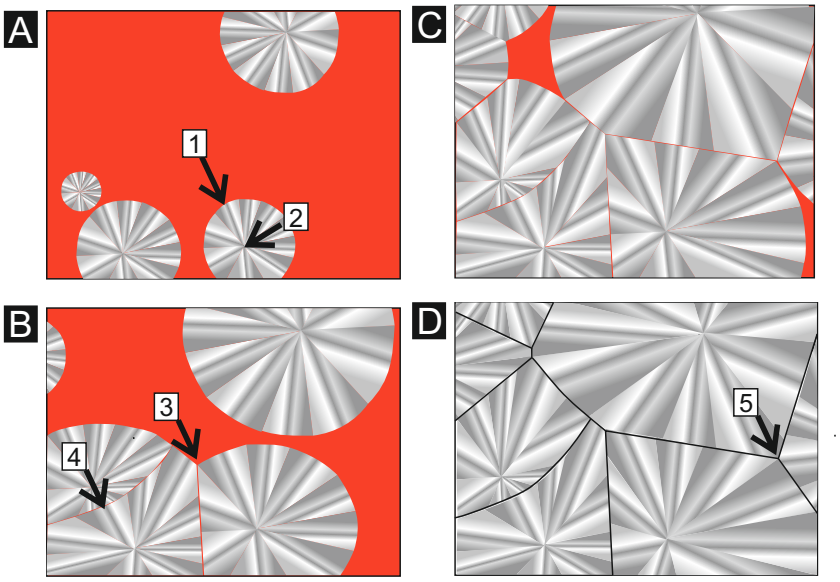

Supplementary figure S 10: Schematic sketch of spherulitic growth on a two dimensional plane containing all the spherulite nuclei. A) Spherulites begin to grow isolated (↑1), and are separated by the adjacent silicate melt from one another. Each spherulite has its own nucleus (↑2). B) Spherulite growth continues so that each spherule growth front begin to impinge on those of neighbouring spherules. Where each spherule growth zone intersects its neighbours', impingement lines form, which can be straight (↑3) or slightly curved (↑4) depending on the spherulite's growth rate during impingement (see text for further detail). C) Spherulite growth continues throughout the melt. D) Spherulite growth ceases after there is no further space for growth. The resulting texture is similar to what we have described before as a honeycomb pattern. These cells can exhibit triple junctions, as described for the texture of the andesitic groundmass (↑5).

As mentioned previously, all textural domains exhibit skeletal augite crystallites (μm to sub-μm size) that emanate radially from a central nucleus, lending the andesitic Izu-Bonin forearc samples a clear spherulitic texture. Spherulitic crystallization in association with alteration below the glass transition temperature is one of the most common explanations for the occurence of spheroidal textures in magmatic and metamorphic rocks (cf. Philpotts, 1977; Sandstå et al., 2011; Fowler et al., 2001). It is still debatable, however, whether spherulitic textures result from devitrification (i.e. secondary crystallization below the glass transition temperature), or from direct primary crystallization from a melt (Monecke et al., 2003). Both processes have been shown to occur under controlled experimental conditions, as well as from observations made in natural samples (Monecke et al., 2003; Fowler et al., 2001; Lofgren, 1974, 1971). However, a clear distinction between primary and secondary spherulitic crystallization is challenging (Monecke et al., 2003; Fowler et al., 2001). A criterion that can be invoked to argue for a magmatic crystallization is the absence of fractures within the spherulites and the surrounding glass, which are often found associated with alteration below the glass transition temperature (GTT – cf. Monecke et al., 2003). In one globule-free sample it is evident that no cracks were formed due to the type of spherulitic crystallization present in the samples of this study. Large degrees of undercooling (> 80 °C below GTT, in the case of plagioclase spherulitic crystallization - Lofgren 1974) are necessary to drive spherulitic crystallization of a magma, and crystallites that form in association with undercooling tend to develop a skeletal shape (Lofgren, 1974; Vetere et al., 2015). Undercooling enables primary spherulitic growth at, or near, isothermal conditions at magmatic temperatures (i.e. above GTT). Spherulitic crystallization was so pronounced in the Izu-Bonin samples that the crystallization fronts of different nuclei collided with each other, forming distinct boundaries that formed a

"honeycomb"-like pattern (cf. Figure S3C and the model in Figure S10). These boundaries comprise a sudden change in the orientation of the crystallites in the space of a few micrometers (see Figure S3C). This spherulitic "honeycomb" pattern often described in the polymer spherulitic crystallization literature (Bassett, 2003; Gránásy et al., 2005; Singfield et al., 2012; Song et al., 2017), and is redolent of spherulitic, variolitic and axiolitic textures of devitrification found in felsic volcanic samples (cf. Cox et al., 1979). Straight impingement lines have been interpreted to indicate equal spherulite growth rates, while curved impingement lines result when two impinging spherulites have grown at slightly different rates (Singfield et al., 2012). As most of the impingement contacts between spherules in our samples are straight, or only slightly curved, it can be concluded that spherulitc growth rates in our samples were similar. We propose that these impingement textures can be further seen as strong evidence for close-to-isothermal, spherulitic crystallization at magmatic temperatures, caused by a strong undercooling of the silicate melt. Although the phenomenon of spherulite impingement is well known in the polymer literature, to the best of our knowledge similar patterns have not been described in natural silicate rocks. Nevertheless, undercooling-assisted spherulitic crystallization, as described in Figures S3C and S4, appears to be consistent with the spherulitic "honeycomb" pattern found in our samples.

References

Bassett D (2003) Polymer Spherulites: A Modern Assessment. Journal of Macromolecular Science, Part B 42(2):227–256

Cox K, Bell J, Pankhurst R (1979) The interpretation of igneous rocks, George Allen and Unwin

Fowler A, Berger B, Shore M, Jones M, Ropchan J (2001) Supercooled rocks: development and significance of varioles, spherulites, dendrites and spinifex in Archaean volcanic rocks, Abitibi Greenstone belt, Canada. Precambrian Research 115(1):311–328

Gránásy L, Pusztai T, Tegze G, Warren JA, Douglas JF (2005) Growth and form of spherulites. Physical Review E 72(1):011605

Ilieva A, Mihailova B, Tsintsov Z, Petrov O (2007) Structural state of microcrystalline opals: A Raman spectroscopic study. Am Mineral 92(8-9):1325–1333

Lafuente B, Downs RT, Yang H, Stone N (2016) The power of databases: the RRUFF project. In: Armbruster T, Danisi R (eds) Highlights in mineralogical crystallography, W. de Gruyter GmbH, pp 1–30

Lofgren G (1971) Spherulitic textures in glassy and crystalline rocks. J Geophys Res 76(23):5635–5648

Lofgren G (1974) An experimental study of plagioclase crystal morphology; isothermal crystallization. American journal of Science 274(3):243–273

Monecke T, Renno AD, Herzig PM (2003) Primary clinopyroxene spherulites in basaltic lavas from the Pacific–Antarctic Ridge. J Volcan Geotherm Res 130(1):51–59

Philpotts AR (1977) Archean variolites – quenched immiscible liquids: Discussion. Can J Earth Sci 14(1):139–144

Saloman EB (2006) Wavelengths, energy level classifications, and energy levels for the spectrum of neutral mercury. Journal of physical and chemical reference data 35(4):1519–1548

Sandstå NR, Robins B, Furnes H, De Wit M (2011) The origin of large varioles in flow-banded pillow lava from the Hooggenoeg Complex, Barberton Greenstone Belt, South Africa. Contrib Mineral Petrol 162(2):365–377

Singfield KL, Chisholm RA, King TL (2012) A Physical Chemistry Experiment in Polymer Crystallization Kinetics. Journal of Chemical Education 89(1):159–162

Song P, Sang L, Zheng L, Wang C, Liu K, Wei Z (2017) Insight into the role of bound water of a nucleating agent in polymer nucleation: a comparative study of anhydrous and monohydrated orotic acid on crystallization of poly (l-lactic acid). RSC Advances 7(44):27150–27161

Vetere F, Iezzi G, Behrens H, Holtz F, Ventura G, Misiti V, Cavallo A, Mollo S, Dietrich M (2015) Glass forming ability and crystallisation behaviour of sub-alkaline silicate melts. Earth-Science Reviews 150:25–44

Wojdyr M (2010) Fityk: a general-purpose peak fitting program. Journal of Applied Crystallography 43(5):1126